

Self-Sensing for Proprioception and Contact Detection in Soft Robots Using Shape Memory Alloy Artificial Muscles

Ran Jing¹, Meredith L. Anderson¹, Juan C. Pacheco Garcia¹, Andrew P. Sabelhaus^{1,2}

Abstract—Estimating a soft robot’s pose and applied forces, also called proprioception, is crucial for safe interaction of the robot with its environment. However, most solutions for soft robot proprioception use dedicated sensors, particularly for external forces, which introduce design trade-offs, rigidity, and risk of failure. This work presents an approach for pose estimation and contact detection for soft robots actuated by shape memory alloy (SMA) artificial muscles, using no dedicated force sensors. Our framework uses the unique material properties of SMAs to self-sense their internal stress, via offboard measurements of their electrical resistance and in-situ temperature readings, in an existing fully-soft limb design. We demonstrate that a simple polynomial regression model on these measurements is sufficient to predict the robot’s pose, under no-contact conditions. Then, we show that if an additional measurement of the true pose is available (e.g. from an already-in-place bending sensor), it is possible to predict a binary contact/no-contact using multiple combinations of self-sensing signals. Our hardware tests verify our hypothesis via a contact detection test with a human operator. This proof-of-concept validates that self-sensing signals in soft SMA-actuated soft robots can be used for proprioception and contact detection, and suggests a direction for integrating proprioception into soft robots without design compromises. Future work could employ machine learning for enhanced accuracy.

I. INTRODUCTION

Robots made from soft materials are commonly claimed to demonstrate safer environmental interactions than their rigid counterparts [1]. For intelligent control of these interactions, it is essential to estimate the robot’s pose, forces, and contact states – a process called *proprioception* [2]. However, these robots’ deformability complicates the integration of proprioceptive sensing [3]. Introducing dedicated force sensors can make the robot more fragile or lessen its natural compliance, which may defeat the purpose of softness [4]. Even when dedicated sensors are well-integrated or are soft themselves, they can be limited to contact detection at one location on the robot [5], add design complexity with additional failure modes [6], or limit manipulation tasks with bulkiness [7], [8]. A robust, integrated solution is still lacking.

This work develops a proprioception approach for a soft robot limb using no additional sensors on the robot dedicated to that task. We exploit a particular type of artificial muscle, the shape memory alloy (SMA) thermoelectric actuator, which can self-sense its stress through electrical resistance measurements [9]. Our insight is that this actuator stress

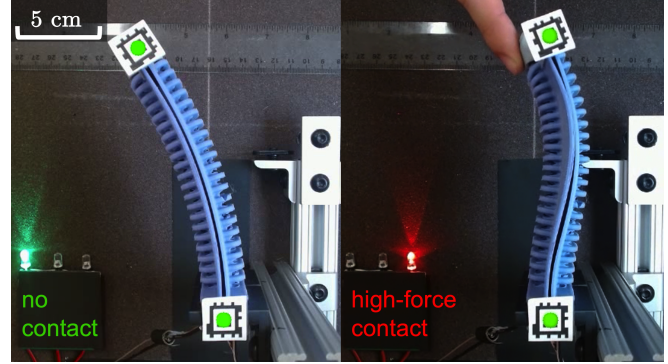


Fig. 1. Our approach, using self-sensing of stress in a soft robot’s artificial muscle actuators, can detect when external contact has occurred. No additional sensors are added to the soft limb’s design.

maps to the soft robot’s pose under no-contact conditions. And if a true pose measurement is available, a difference between predicted vs. measured pose indicates that the robot has deformed under an external load (Fig. 1), thus detecting contact anywhere on the robot’s body.

This paper contributes a proof-of-concept for this self-sensing of internal stress and external contact in an SMA-based soft robot limb. Our scientific contributions demonstrate that electrical resistance of the thermoelectric SMA wire (when below its critical transition temperature) deconflicts the hysteresis in actuator temperature versus stress. Additionally, we show that resistance is comparable to a temperature signal during contact detection. Given a simple polynomial data fit as an estimator, we show pose errors of 15.3% throughout the full operating range of the SMAs (up to 160° C), and contact force prediction errors of ≈ 0.02 N when below their critical transition temperature (90° C).

A. Existing Approaches in Proprioception

State-of-the-art in estimating a soft robot’s pose and external loads commonly uses either dedicated sensors or bulky external hardware. Dedicated sensors can be traditionally rigid and more mature, or softer and more exploratory, whether resistive [10], capacitive [11], [12], ionic [13], magnetic [14], or optical [15]–[17], among many others. These have been used in combination with both finite-element models [10] and machine learning [18], [19], [19]–[21] to estimate internal stresses or pose. However, these approaches may require multiple sensors to infer properties of the whole robot [16] due to their localized readings, and may increase rigidity at each location. Increasing sensor density and surface area can address the issue [22], but at the cost of design tradeoffs.

¹R. Jing, M.L. Anderson, J.C. Pacheco Garcia, and A.P. Sabelhaus are with the Department of Mechanical Engineering, Boston University, Boston MA, USA. {rjing, merland, jcp29, asabelha}@bu.edu. ²A.P. Sabelhaus is also with the Division of Systems Engineering, Boston University, Boston MA, USA.

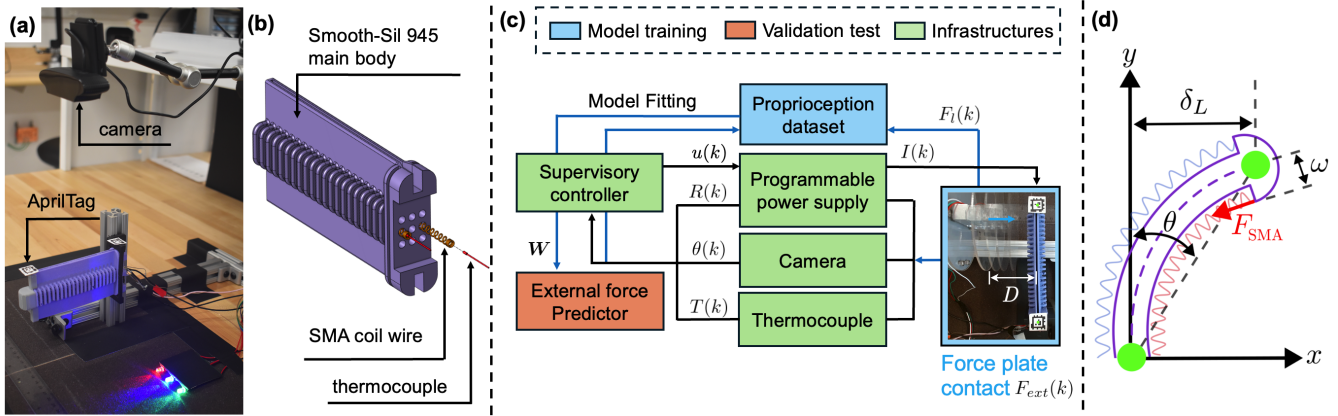


Fig. 2. Architecture overview. Our existing limb design uses (a) computer vision for ground truth measurements of the robot’s pose, where the limb includes (b) a silicone body actuated by shape memory alloy wire coils with a thermocouple affixed at the base. (c) Our data-driven approach includes our prior work in temperature-safe feedback control of these thermal SMA wires, with a data collection and sensing setup. (d) Our free-motion contact model uses a simple beam-bending approximation to map pose to actuator stress.

External sensors can also be used to determine the pose of a soft robot and its contact forces, commonly via RGB-D cameras or motion trackers [23] [24]. These high-quality measurements can similarly be used with either finite element models [25] or kinematic approximations [26] for pose and force estimation. However, these techniques are not *proprioception* in spirit, since proprioception implies sensors internal to the robot’s body [2], and are therefore limited to predetermined and controlled environments.

B. Actuator Self-Sensing and Proprioception

Another method for proprioception is to use actuators that also serve as sensors, known as *self sensing* [27]. Self-sensing requires fewer design constraints than dedicated sensors, even possibly no additional onboard hardware. Dielectric elastomer actuators can self-sense via electrical changes versus deformation [28], and liquid crystal elastomer actuators have a correlation between deformation and temperature [29], both allowing pose estimates of a soft robot. However, both DEAs and LCEs face challenges in practical applications due to e.g. low force output, large driving voltages [30], or slow speeds. For pneumatic bellows, internal pressure sensors can be used to infer contact [2], [31] but rely on bulky designs of pumps and valves.

C. Shape Memory Alloy Actuator Self-Sensing and Soft Robot Integration

Alternatively, shape memory alloy (SMA) artificial muscle actuators can be high force [32] and high speed [33], [34] with easy low-voltage integration onboard a soft robot [35]. SMA actuators generate force by a reversible material-phase transformation when subjected to thermal stimuli. More importantly, SMAs can self-sense, as stress and strain relate to their temperature and material phase. Prior work has demonstrated that under controlled lab conditions, SMA self-sensing can predict the actuator’s displacement [36]–[40] or the force it applies to a mechanism [41], [42], even enabling pose control via self-sensing [43]. However, these approaches struggle to translate to robots outside of precision test setups.

Our past work demonstrated that it is possible to integrate in-situ temperature measurements of SMAs in a soft robot, eliminating such test setups [44], [45]. We demonstrated pose predictions under no-load conditions [44], [45], though with limited accuracy due to hysteresis [46]. However, it is known that electrical resistance of an SMA changes with its material phase [47], introducing an additional signal which could de-conflict hysteresis and predict stress. To our knowledge, no prior work has integrated SMA stress self-sensing into a soft robot limb for proprioception and external contact detection.

D. Approach and Outlook

The remainder of this manuscript outlines our mathematical setup of our problem, hardware prototype, modeling approach, and testing. We hypothesize that adding electrical resistance measurements of the SMA during operation will enable full proprioception. We first validate pose estimation via actuator stress self-sensing, with no contact, before presenting contact detection as a separate question. Our results are achieved using a simple least-squares polynomial fit to the self-sensing signals, prompting future work in machine learning techniques to improve contact prediction accuracy.

We utilize a computer vision system as a stand-in for in-situ pose measurements, which were previously obtained via a soft bending sensor in our existing designs [45], in order to reduce error and focus on our hypothesis of the SMA resistance self-sensing relationship. However, since much of our past work [48] and others [49] contains such pose sensors as standard practice, we anticipate that our framework can be applied with only these already-onboard sensors.

II. SOFT ROBOT LIMB ARCHITECTURE

Since we hypothesize that self-sensing proprioception and contact detection is possible without design changes to a soft robot that uses SMA artificial muscles, this paper uses such a robot from our prior work [32], [45] (Fig. 2(a)-(b)). No additional on-board sensors are added.

A. Actuator and Existing Sensors Design

The existing prototype consists of a limb cast from silicone rubber (Fig. 2(b)) that allows high force and rapid motion in a 2D plane. The limb contains a set of SMA wire coils (Dynalloy Flexinol 90°C, 0.020" diam.) along each edge, which when heated via Joule heating through electric current, contract and cause bending. We use a programmable power supply to apply a voltage per-actuator, taken as the control input to the robot ($\mathbf{u} = V$), inducing corresponding currents i which are recorded to a computer from the power supply. In this paper, we isolate the limb to unidirectional motion with only a single actuator ($u \in \mathbb{R}^+$). Using this commanded voltage and current reading from the power supply, we calculate a discrete-time series of resistance signals as the robot operates, $R(k) = V(k)/i(k)$. We note that the resistance reading is therefore offboard and does not require a dedicated sensor in the robot.

Our prior manuscripts detail the computer vision system via AprilTags [50], which calculates a bending angle $\theta(k)$, and a thermocouple at the base of the robot which reads an estimate $T(k)$ of the SMA's temperature [44]. Our most recent work [32] has also integrated a force plate for external ground truth measurements of the limb's contact with an environment, $F_{ext}(k)$, so our datasets include K -many points $\{R(k), \theta(k), T(k), F_{ext}(k)\}^K$.

B. Control System

To calculate the input signals $u(k)$, we use a model-based temperature controller that monitors a nominal $u_{nom}(k)$, ensuring the robot does not overheat [51] during data collection i.e. "motor babbling" as u_{nom} (Fig. 2(c)). The temperature dynamics, extensively validated by our group, can be approximated as an affine scalar system, $T_{k+1} = a_1 T_k + a_2 u_k + a_3$. We calibrate this model using our approach from [32].

The supervisory controller ensures that temperatures remain below a maximum, $T(k) < T^{MAX}$. To do so, we dynamically saturate the input u_{nom} via $u(k) = \min(u_{nom}(k), \gamma u^*(k))$, where $\gamma \in (0, 1]$ is a discount factor for conservativeness. The dynamic saturation limit is $u^*(k) = \frac{1}{a_2} (T_{adj}^{MAX} - a_1 T(k) - a_3)$ and the discounted maximum temperature is $T_{adj}^{MAX} = (1/\gamma - a_1((1-\gamma)/\gamma))T_{max} - a_3((1-\gamma)/\gamma)$, required as part of a proof of stability and invariance of the closed-loop system [51].

III. ACTUATOR FORCE SELF-SENSING

Our first experiment tests the hypothesis that electrical resistance, together with *in-situ* temperature measurements, can predict the robot's pose without hysteresis.

A. Pose Proprioception Hypothesis

Shape memory materials actuate via temperature change. It is well-known [52]–[54] that the mechanics of induced stress in SMAs can be well-modeled as a lumped parameter system with four variables: $\sigma = f(\epsilon, T, \xi)$. Here, σ is stress in the material, ϵ is strain, T is temperature, and $\xi \in [0, 1]$ is the phase fraction of austenite vs. martensite [40]. Although the material phase ξ is difficult to measure, much prior work

has demonstrated [47], [55]–[58] that the electrical resistance R of SMAs varies with ξ . In addition, since our SMA coils have no appreciable cross-sectional area change, their applied force is $F_{SMA} \propto \sigma$. Proprioception could occur, therefore, if a function $f(\cdot)$ exists so that $F_{SMA} = f(\epsilon, T, R)$.

B. No-Contact Artificial Muscle Actuator Force Model

We observe that in the case of no external contact on the limb, and under static equilibrium, the limb's bending angle $\theta(k)$ is uniquely determined by $F_{SMA}(k)$. Furthermore, under the assumption of constant-curvature deformation in a soft robot [59], the limb's bending angle θ has a one-to-one geometric relationship with the strain ϵ of the SMA.

Our prior work has shown that a simple Euler-Bernoulli beam bending model sufficiently models this deformation for an SMA-powered soft limb [48]. Here, the SMA connection at the distal edge of the limb creates a moment at the tip. The tip displacement at time k of $\delta_L(k) = L \sin^2(\theta(k))/\theta(k)$, determined by trigonometry of a constant-curvature arc (Fig. 2(d)). With a distance of w between the SMA's attachment point and the limb's centerline, Euler-Bernoulli beam mechanics admit the analytical relationship:

$$F_{SMA} = \left(\frac{4EI}{L^2 w} \right) \delta_L = \left(\frac{4EI}{Lw} \right) \left(\frac{\sin^2(\theta)}{\theta} \right), \quad (1)$$

where E and I are the elastic modulus and area moment of inertia of the robot as a beam, and L is limb's length.

Observe that eqn. (1) is a function of only the limb bending angle θ under free motion. By defining the constant $\zeta = 4EI/(L^2 w) \in \mathbb{R}$, eqn. (1) for timestep k can be written as $F_{SMA}(k) = \zeta \sin^2(\theta(k))/\theta(k)$.

For our prototype, the calibrated angle-to-stress coefficient is $\zeta = 4.1767N/rad$, using $E = 1.79N/(mm^2)$, $L = 105mm$, and $w = 3.5mm$, via geometry and material specifications for Smooth-Sil 945, and $I = bh^3/12$, where the limb's rectangular cross section is $b = 60mm$ $h = 3.5mm$. The model predicts 1.06N of the muscle force of the SMA when the bending angle is 15°, matching the experimental results in [32] with a prediction error less than 10%.

C. Muscle Force and Limb Pose Estimation using SMA State

Eqn. (1) suggests that predicting the pose $\theta(k)$ is equivalent to predicting the SMA force F_{SMA} under no-contact, and that θ determines strain ϵ . We therefore seek a function $F_{SMA} = g(T, R)$, where F_{SMA} is calculated from a measured θ , simplifying the hypothesis.

Since the first-principles relationship between σ , T , and R is complicated and highly nonlinear, we decide to take a data-driven approach to determine an estimator $\hat{F}_{SMA} = g(T, R)$. We collect a set of datapoints $d_f = \{\theta, T, R\}$ tuples during free movement of the limb, and convert to $\{F_{SMA}, T, R\}$ via eqn. (1). To create these motions, we generate the motor babbling signal u_{nom} from Sec. II-B as PI feedback on randomly selected bending angle setpoints, $\bar{\theta}$, as in [44], with a temperature limit $T_{MAX} = 135^\circ C$, justified by our recent work [32]. We chose ten setpoints between $10^\circ < \bar{\theta} < 40^\circ$

with multiple trials for a total dataset of $D_f = \{d_f(k) | k = 1 \dots 600\}$ points.

Inspecting the collected data, we observe highly different $\{T, R\} \rightarrow F_{SMA}$ relationships at low temperatures versus high temperatures, diverging around $\approx 100^\circ\text{C}$ (blue vs. orange in Fig. 3), which is around the critical transition temperature for our Nitinol alloy. Visually, the relationship appears linear below that point, and quadratic afterwards. We therefore manually split the dataset into $D_{cold} = \{d_f(k) | (T(k) < 100^\circ\text{C}) \wedge (R(k) > 1.7\Omega)\}$, and $D_{hot} = D_f \setminus D_{cold}$, and consider polynomial curve fits of various degrees for both sets alongside a switching strategy.

For a prediction using an m -degree polynomial at some test point $\mathbf{x} = [T, R]^\top$, we construct an extended vector $\mathbf{X}_m^e = \mathcal{L}(\mathbf{x}, m) \in \mathbb{R}^{N_m \times 1}$. The operator \mathcal{L} generates a vector of monomials of the form $[x_m^e]$, where $\{x_m^e = x_1^p x_2^q \dots x_m^z, p, q, \dots, z | \text{sum}(p, q, \dots, z) = 0, \dots, m\}$. For instance, with a quadratic fit ($m = 2$), then $\mathbf{X}_2^e = [1, T, R, TR, T^2, R^2]^\top$. Then, given a vector of weights for each monomial, $\mathbf{W} \in \mathbb{R}^{N_m \times 1}$, the polynomial prediction is $\hat{F}_{SMA} = \mathbf{W}^\top \mathbf{X}_m^e$. To find the weights \mathbf{W} for a dataset $D_j = \{d_f(1) \dots d_f(J)\}$, we calculate $\mathbf{F}_{SMA} = [F_{SMA}(1), \dots, F_{SMA}(J)]^\top$ from eqn. (1) and extended state matrix of all datapoints as $\mathbf{M}_m^e = [\mathbf{X}_m^e(1), \dots, \mathbf{X}_m^e(J)]^\top \in \mathbb{R}^{J \times N_m}$. The least-squares fit is then $\mathbf{W} = (\mathbf{M}_m^e)^\dagger \mathbf{F}_{SMA}$, where \dagger is the pseudoinverse. Applying this approach to D_{hot} and D_{cold} with $m = \{1, 2\}$ with gives the weights \mathbf{W}_{hot} and \mathbf{W}_{cold} . Our predictor over the whole state space is then

$$\hat{F}_{SMA}(\mathbf{x}) = \begin{cases} \mathbf{W}_{cold}^\top \mathbf{X}_m^e & \text{if } T < 100^\circ \wedge R > 1.7\Omega \\ \mathbf{W}_{hot}^\top \mathbf{X}_m^e & \text{else} \end{cases} \quad (2)$$

D. Experimental Result

Using a standard 3-fold cross validation, we obtained the \mathbf{W}_{hot} and \mathbf{W}_{cold} plotted as polynomial surfaces in Fig. 3, showing that a linear fit ($m = 1$) is acceptable for D_{cold} but quadratic is needed for D_{hot} , and therefore $m = 2$ is used in the validation test. A snapshot of time-series predictions over a test set in Fig. 4 visually confirms the quality of these actuator force (i.e., robot pose) predictions. With the prediction error denoted $e(k) = \hat{F}_{SMA}(k) - F_{SMA}(k)$, the average error was $\bar{e} = \sum_k e(k) / (K - 1) = 0.118\text{N}$, which normalized as a percent was $\bar{e}_p = \sum_k e(k) / (F(k)(K - 1)) = 15.28\%$. This is significantly improved over our prior work without resistance self-sensing [44], [46].

IV. CONTACT FORCE ESTIMATION

For manipulation or locomotion tasks in soft robotics, estimation of external applied forces may be just as important as the robot's pose. We have shown above that when the robot's pose change is only due to internal actuator stress, F_{SMA} , the mechanics can be accurately learned from self-sensing alone as $\hat{F}_{SMA} = g(T, R)$, where our proof-of-concept $g(\cdot)$ is eqn. (2). However, upon the addition of an external load F_{ext} anywhere along the robot, the beam bending equations become statically indeterminate: the displacement $\delta_L(\theta)$ from eqn. (1) becomes $\delta_L(\theta, F_{ext})$. We

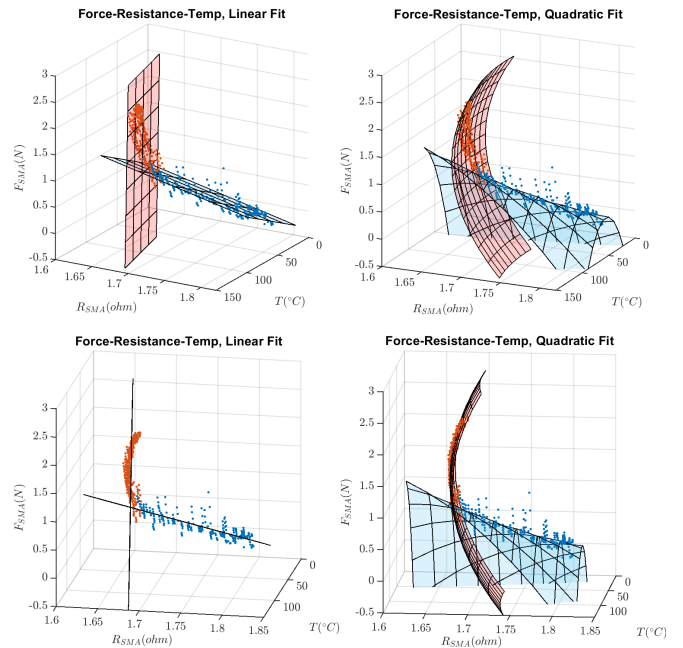


Fig. 3. Both linear and quadratic regression models for no-contact actuator force self-sensing demonstrate that resistance deconflicts temperature hysteresis, given a split between hot (orange) and cold (blue) operating ranges per the SMA's critical transition temperature.

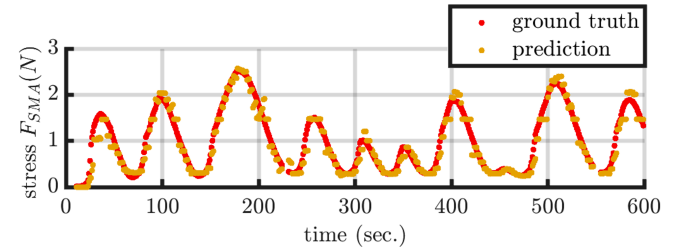


Fig. 4. A snapshot of no-contact actuator force predictions shows a realistic trend using only self-sensing of resistance and in-situ temperature readings.

therefore hypothesized that given an additional signal of the robot's pose (i.e., θ from another internal sensor), sufficient information exists to predict F_{ext} during contact.

A. Contact Force Prediction model

In this setting, we now seek to predict the external force F_{ext} from system state $\mathbf{x} = [T, R, \theta]^\top$, in other words, a function $f(\cdot)$ such that $\hat{F}_{ext} = f(T, R, \theta)$. Motivated by the positive results during no-contact, we consider again polynomial fits on \mathbf{x} . Assume we want to derive a predictor using a dataset of motions that now contains intermittent environmental contact, $D_c = \{F_{ext}(k), T(k), R(k), \theta(k)\}, k = 1 \dots K$. As in Sec. III-C, a m -degree polynomial prediction uses the extended state vector $\mathbf{X}_m^e = \mathcal{L}(\mathbf{x}, m)$ now with our $\mathbf{x} = [T, R, \theta]^\top$. The prediction is $\hat{F}_{ext}(\mathbf{x}) = \mathbf{W}^\top \mathbf{X}_m^e$. And as before, we can calculate the weights per least-squares, arranging the dataset as $\mathbf{F}_{ext} = [F_{ext}(1), \dots, F_{ext}(K)]^\top$ and $\mathbf{M}_m^e = [\mathbf{X}_m^e(1), \dots, \mathbf{X}_m^e(K)]^\top$. The fit is then $\mathbf{W} = (\mathbf{M}_m^e)^\dagger \mathbf{F}_{ext}$. For this setting, we extrapolate that a polynomial of $m = 3$ is appropriate, since $\mathbf{x} \in \mathbb{R}^3$ now.

B. Contact Force Dataset and Model Fitting

We generate a such data set D_c using the external force plate setup from [32], per the procedure in Fig. 2(c). The force plate was positioned parallel to the soft limb at four fixed distances from the tip’s neutral position, $\delta_L^{MAX} = \{20, 30, 40, 50\}mm$. We select four different SMA temperature limits $T^{MAX} = \{85, 100, 115, 130\}^\circ C$, motivated by the no-contact observation that resistance relationships change qualitatively around $90\text{-}100^\circ C$. For each parameter combination, we manually design the u_{nom} control signal’s hold times at various $\bar{\theta}$ to span the state space of \mathbf{x} as broadly as possible. We kept a small amount of current ($i > 0.2A$) at all times for our resistance calculation to be valid. With 16 different parameter settings, we obtained over 400 minutes of active robot motion, for $K = 24,000$ datapoints.

To test our hypothesis, we again use 3-fold cross validation on D_c . However, we now split each training set into three separate models with different combinations of self-sensing states, to compare the benefits of including resistance measurements: $\{R, T, \theta\}$, $\{R, \theta\}$ and $\{T, \theta\}$.

C. Experimental Results

Table I shows the average prediction error of the three external force predictors using our cubic polynomial fit ($m=3$) on the same testing set, and Fig. 5 shows a snapshot of the models applied to the test set.

TABLE I
AVG. EXTERNAL FORCE PREDICTION ERRORS

Self-Sensing Signal Combination:	$\{R, T, \theta\}$	$\{R, \theta\}$	$\{T, \theta\}$
Avg. Prediction Error (N):	0.0247	0.0250	0.0620

The overall results demonstrate that external force estimation is indeed possible with our self-sensing signals. Visually, both $\{R, T, \theta\}$ and $\{T, \theta\}$ have high-quality force proprioception. Statistically, including resistance may lower the error during no-contact predictions, but visually in Fig. 5, there is little benefit (c.f. green versus orange time series). Removing temperature signals appears to increase errors, yet all predictors seem to register nonzero values similarly to ground truth. It is uncertain if this inconclusive result arises from our simplistic choice of estimator, or from the underlying physics of the problem. Future work is needed to investigate the unsolved questions we mentioned above.

V. CONTACT DETECTION AND OPERATIONAL LIMITS

This manuscript’s goal is validation of electrical resistance as a self-sensing signal for SMA-based soft robot proprioception, rather than an advanced predictor of F_{ext} . However, we have observed nonzero contact forces in similar cases among all three predictors, so it may be possible that resistance is interchangeable with temperature in limited settings. We therefore evaluate if a binary contact vs. no-contact state prediction is possible with self-sensing. Along the way, we contribute a surprising discovery about our shape memory actuator: the limit where resistance is interchangeable with temperature also happens to be approximately the critical transition temperature (about $90^\circ C$ for our Nitinol).

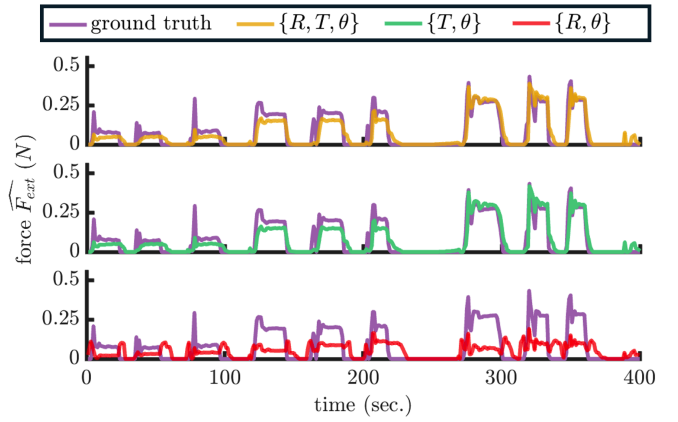


Fig. 5. External force estimation with self-sensing signals shows that including electrical resistance R in addition to temperature and pose (T, θ) has minimal improvement. However, we notice that the R, θ model predicts nonzero forces at similar times as those with temperature, prompting the question: can R substitute T for contact detection?

A. Binary Contact Detection and Calibration

As a simple test, we introduce a classifier for binary detection of contact ($C = 1$) or no contact ($C = 0$) of the soft limb against an environment, using a threshold on the estimated external force: $C = \{1 \text{ if } \hat{F}_{ext} > F_{thresh}, \text{ else } 0\}$. We then seek to find an optimal F_{thresh} for different \hat{F}_{ext} models, and use the optimal classifiers to compare test statistics on C . However, since electrical resistance appears to saturate around a certain temperature, this question is deeply intertwined with selecting a maximum temperature T^{MAX} which is valid for each model.

We propose a data-driven procedure to iteratively determine F_{thresh} and T^{MAX} , serving as a calibration method for the classifier, focusing on resistance as a substitute for temperature. We run a series of regressions, selecting sub-datasets per temperature limit: $D_s(T^{MAX}) = \{d(k) | T(k) \in [0, T^{MAX}]\}$. We pick different T^{MAX} between $[60, 130]^\circ C$ with a step size of 5° to build subsets, and cross-validate.

Fig. 6(a) shows that electrical resistance can be used in place of temperature, $\{T, \theta\}$ versus $\{R, \theta\}$, for similar-quality F_{ext} predictions up to a clear limit on temperature. It was surprising that this T^{MAX} coincided almost exactly with the no-contact scenario, and with the critical transition temperature: $90^\circ C$. We therefore focus on $\{R, \theta\}$ vs. $\{T, \theta\}$ models only below this operational limit of $90^\circ C$.

Next, we select the optimal threshold F_{thresh}^* by sweeping over a range of F_{thresh} values, calculating classification statistics for each, and picking a pointwise maximum. We use the standard statistical metrics of precision and recall to evaluate how well a contact detector matches the ground truth: $Pre = TP/(TP + FP)$ and $Rec = TP/(TP + FN)$, where TP is true positive, and FP (N) is false positive (negative). Since there is a trade-off between precision and recall, we also calculate the F1-score, where $F1 = 2Pre * Rec / (Pre + Rec)$. Fig. 6(b) shows how the F1 score, precision and recall evolves as the contact threshold increases (only considering $T^{MAX} = 90^\circ C$). From the curve in Fig. 6, we set $F_{thresh}^* = \text{argmax } F1(F_{thresh})$, i.e., the threshold with the largest F1

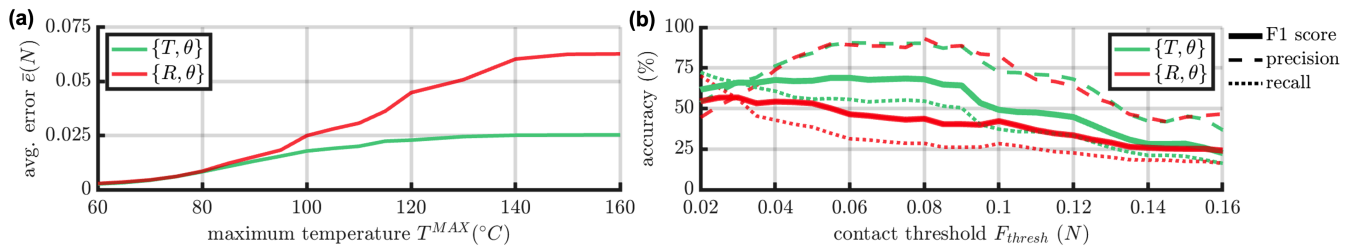


Fig. 6. Contact force estimation errors are comparable between the self-sensing signals of temperature and pose $\{T, \theta\}$ versus electrical resistance and pose $\{R, \theta\}$ up to the $90^{\circ}C$ critical transition temperature of the SMA (a). Under this operational limit, a binary contact detector can be optimally calibrated with a simple threshold F_{thresh} by taking the maximum of some statistic, e.g., F1 score or precision (b).

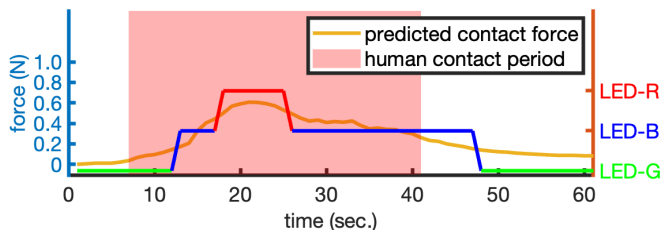


Fig. 7. A demonstration for the human contact experiment and curves showing real-time model prediction and LED indication.

score. In our test, $\max(F1)$ occurs at $F_{thresh}^* = 0.04$ N.

Table II shows these three metrics for F_{thresh}^* , and as a comparison, the precision-optimal threshold at $F_{thresh} = 0.08$ N. In both cases and as is visible in Fig. 6(b), the precision is similar between both $\{R, \theta\}$ and $\{T, \theta\}$, yet recall suffers slightly with R , causing a correspondingly lower F1 score.

TABLE II
CONTACT CLASSIFIER PREDICTION STATISTICS

Signals	F_{thresh}	Precision (%)	Recall (%)	F1 (%)
$\{T, \theta\}$	0.04N	76.24	60.73	67.61
$\{R, \theta\}$	0.04N	73.79	42.94	54.29
$\{T, \theta\}$	0.08N	90.28	54.92	68.06
$\{R, \theta\}$	0.08N	93.15	31.40	46.97

B. Real-time external contact detection

Finally, we implemented the contact detector on hardware for a real-time detection demonstration. This time, instead of the rigid force plate in the data collection stage, a human user pushed on the robot with their finger, and an LED lights up depending on contact state (Fig. 1). This test used the $\{R, T, \theta\}$ estimate of \hat{F}_{ext} as a demonstration. In addition to the binary classifier for no contact (green) versus contact (blue), we added a threshold for high-force contact (red), calculated via our method as $0.1N$ and $0.5N$ respectively. Fig. 7 provides a representative example of our human contact detector, demonstrating realistic behavior, though a delay occurs after the human removes their contact.

VI. DISCUSSION, CONCLUSION, AND FUTURE WORK

This paper demonstrates that electrical resistance self-sensing signals enable pose proprioception for an SMA-based soft robot limb, and complement existing signals when estimating external applied forces. Using very simple

polynomial regression models and a thresholding binary classifier, we show that it is possible to detect when a human contacts such a robot in real-time. We propose a procedure to estimate the operational range of possible contact predictors, and a calibration scheme for the contact predictor.

This exploratory study validates our self-sensing concept, yet much work remains in practical implementation and accuracy improvements. In particular, we have utilized ground-truth measurements (a computer vision system) for both training and as a signal during external force estimation. Though it is standard practice to use CV in lab settings [13], work is underway to test these approaches with an existing prototype that includes an internal capacitive bending sensor that replaces the computer vision signal, creating true proprioception. Additionally, our test conditions only included contact at one location in the robot. Since our contact detection method did not make any assumptions about contact location, we plan to extend our tests to multi-contact settings.

Our approach demonstrates proof-of-concept force proprioception, but accuracy has room for improvement. We believe that this misalignment could be improved by applying more advanced machine learning tools on our dataset, e.g., LSTMs [44] or DNNs [19]. These same methods may be necessary for multidirectional bending of the limb, or the use of multiple SMA muscles simultaneously.

Similarly, our results for estimating external forces F_{ext} are inconclusive about the benefit of self-sensing electrical resistance in addition to temperature in-situ for SMA muscles. It is unclear whether this is a limitation of our test setup and data collection (for example, if temperature was already too strongly correlated with contact), or with the choice of predictor (for example, if we were underfitting), or is a true physical phenomenon. Future investigations will isolate this question by statistical analysis of the dataset, and learning models with larger numbers of parameters.

Finally, our future work will deploy an improved version of our proprioception method in human-robot collaboration tasks, where contact forces could be detected and limited to prevent injury to a human user.

REFERENCES

- [1] D. Rus and M. T. Tolley, "Design, fabrication and control of soft robots," *Nature*, vol. 521, no. 7553, p. 467–475, May 2015.

- [2] Y. Toshimitsu, K. W. Wong, T. Buchner, and R. Katzschmann, "SoPrA: Fabrication & Dynamical Modeling of a Scalable Soft Continuum Robotic Arm with Integrated Proprioceptive Sensing," in *2021 IEEE/RSJ International Conference on Intelligent Robots and Systems (IROS)*, Sept. 2021, pp. 653–660.
- [3] M. McCandless, F. J. Wise, and S. Russo, "A Soft Robot with Three Dimensional Shape Sensing and Contact Recognition Multi-Modal Sensing via Tunable Soft Optical Sensors," in *2023 IEEE International Conference on Robotics and Automation (ICRA)*, May 2023, pp. 573–580. [Online]. Available: <https://ieeexplore.ieee.org/abstract/document/10160877>
- [4] A. Alian, G. Mylonas, and J. Avery, "Soft continuum actuator tip position and contact force prediction, using electrical impedance tomography and recurrent neural networks," in *2023 IEEE International Conference on Soft Robotics (RoboSoft)*, 2023, pp. 1–6.
- [5] T. Hellebrekers, O. Kroemer, and C. Majidi, "Soft Magnetic Skin for Continuous Deformation Sensing," *Advanced Intelligent Systems*, vol. 1, no. 4, p. 1900025, 2019. [Online]. Available: <https://onlinelibrary.wiley.com/doi/abs/10.1002/aisy.201900025>
- [6] T. G. Thuruthel, B. Shih, C. Laschi, and M. T. Tolley, "Soft robot perception using embedded soft sensors and recurrent neural networks," *Science Robotics*, vol. 4, no. 26, p. eaav1488, 2019. [Online]. Available: <https://www.science.org/doi/abs/10.1126/scirobotics.aav1488>
- [7] M. McCandless, A. Perry, N. DiFilippo, A. Carroll, E. Billatos, and S. Russo, "A soft robot for peripheral lung cancer diagnosis and therapy," *Soft Robot.*, vol. 9, no. 4, pp. 754–766, Aug. 2022.
- [8] D. Van Lewen, C. Wang, H. C. Lee, A. Devaiah, U. Upadhyay, and S. Russo, "Capacitive Origami Sensing Modules for Measuring Force in a Neurosurgical, Soft Robotic Retractor," in *2024 IEEE International Conference on Robotics and Automation (ICRA)*, May 2024, pp. 5302–5308. [Online]. Available: <https://ieeexplore.ieee.org/abstract/document/10610863>
- [9] J. Prechtl, S. Seelecke, P. Motzki, and G. Rizzello, "Model-based, self-sensing actuator system based on antagonistic sma wires," in *ACTUATOR: International Conference and Exhibition on New Actuator Systems and Applications 2021*, 2021, pp. 1–4.
- [10] S. Tian, B. G. Cangan, S. E. Navarro, A. Beger, C. Duriez, and R. K. Katzschmann, "Multi-tap resistive sensing and fem modeling enables shape and force estimation in soft robots," *IEEE Robotics and Automation Letters*, vol. 9, no. 3, pp. 2830–2837, 2024.
- [11] R. K. Kramer, C. Majidi, R. Sahai, and R. J. Wood, "Soft curvature sensors for joint angle proprioception," in *2011 IEEE/RSJ International Conference on Intelligent Robots and Systems*. IEEE, 2011, pp. 1919–1926.
- [12] A. Atalay, V. Sanchez, O. Atalay, D. Vogt, F. Haufe, R. J. Wood, and C. J. Walsh, "Batch Fabrication of Customizable Silicone-Textile Composite Capacitive Strain Sensors for Human Motion Tracking," *Advanced Materials Technologies*, 2017.
- [13] M. Annabestani, B. Kamare, M. Shabani, S. V. Magalhaes, A. Mondini, and B. Mazzolai, "A bioinspired multifunctional soft gripper with embedded sensing ability: a potential way for sustainable agricultural harvesting," in *2023 IEEE International Workshop on Metrology for Agriculture and Forestry (MetroAgriFor)*, 2023, pp. 182–187.
- [14] Y. Yue, Y. Tang, Q. Wang, W. Xiao, J. Liu, J. Wang, M. Chen, G. Wu, and B. Su, "Active Perception in Non-Visual Recognition Environments by Stretchable Tentacle Sensor Arrays," *ACS Applied Materials & Interfaces*, vol. 14, no. 23, pp. 26913–26922, June 2022. [Online]. Available: <https://doi.org/10.1021/acsmi.2c04717>
- [15] Y. She, S. Q. Liu, P. Yu, and E. Adelson, "Exoskeleton-covered soft finger with vision-based proprioception and tactile sensing," in *2020 IEEE International Conference on Robotics and Automation (ICRA)*, 2020, pp. 10075–10081.
- [16] B. Kim, J. Ha, F. C. Park, and P. E. Dupont, "Optimizing curvature sensor placement for fast, accurate shape sensing of continuum robots," in *2014 IEEE International Conference on Robotics and Automation (ICRA)*, May 2014, pp. 5374–5379.
- [17] O. Faris, R. Muthusamy, F. Renda, I. Hussain, D. Gan, L. Seneviratne, and Y. Zweiri, "Proprioception and exteroception of a soft robotic finger using neuromorphic vision-based sensing," *Soft Robotics*, vol. 10, no. 3, pp. 467–481, 2023.
- [18] K. Chin, T. Hellebrekers, and C. Majidi, "Machine Learning for Soft Robotic Sensing and Control," *Advanced Intelligent Systems*, vol. 2, no. 6, p. 1900171, 2020. [Online]. Available: <https://onlinelibrary.wiley.com/doi/abs/10.1002/aisy.201900171>
- [19] R. L. Truby, C. Della Santina, and D. Rus, "Distributed proprioception of 3d configuration in soft, sensorized robots via deep learning," *IEEE Robotics and Automation Letters*, vol. 5, no. 2, pp. 3299–3306, 2020.
- [20] G. Soter, A. Conn, H. Hauser, and J. Rossiter, "Bodily aware soft robots: Integration of proprioceptive and exteroceptive sensors," in *2018 IEEE International Conference on Robotics and Automation (ICRA)*, 2018, pp. 2448–2453.
- [21] B. W. K. Ang and C.-H. Yeow, "A Learning-Based Approach to Sensorize Soft Robots," *Soft Robotics*, May 2022. [Online]. Available: <https://www.liebertpub.com/doi/full/10.1089/soro.2020.0172>
- [22] C. Lin, H. Zhang, J. Xu, L. Wu, and H. Xu, "9dtact: A compact vision-based tactile sensor for accurate 3d shape reconstruction and generalizable 6d force estimation," *IEEE Robotics and Automation Letters*, 2023.
- [23] C. Della Santina, R. K. Katzschmann, A. Biechi, and D. Rus, "Dynamic control of soft robots interacting with the environment," in *2018 IEEE International Conference on Soft Robotics (RoboSoft)*, 2018, pp. 46–53.
- [24] R. K. Katzschmann, C. D. Santina, Y. Toshimitsu, A. Biechi, and D. Rus, "Dynamic motion control of multi-segment soft robots using piecewise constant curvature matched with an augmented rigid body model," in *2019 2nd IEEE International Conference on Soft Robotics (RoboSoft)*, 2019, pp. 454–461.
- [25] Z. Zhang, A. Petit, J. Dequidt, and C. Duriez, "Calibration and external force sensing for soft robots using an rgb-d camera," *IEEE Robotics and Automation Letters*, vol. 4, no. 3, pp. 2356–2363, 2019.
- [26] C. Della Santina, R. L. Truby, and D. Rus, "Data-Driven Disturbance Observers for Estimating External Forces on Soft Robots," *IEEE Robotics and Automation Letters*, vol. 5, no. 4, pp. 5717–5724, Oct. 2020.
- [27] U. Gupta, L. Qin, Y. Wang, H. Godaba, and J. Zhu, "Soft robots based on dielectric elastomer actuators: a review," *Smart Materials and Structures*, vol. 28, no. 10, p. 103002, sep 2019. [Online]. Available: <https://dx.doi.org/10.1088/1361-665X/ab3a77>
- [28] J. Prechtl, M. Baltes, K. Flaßkamp, and G. Rizzello, "Sensorless proprioception in multi-dof dielectric elastomer soft robots via system-level self-sensing," *IEEE/ASME Transactions on Mechatronics*, pp. 1–12, 2024.
- [29] J. Wu, W. Ye, Y. Wang, and C.-Y. Su, "Modeling based on a two-step parameter identification strategy for liquid crystal elastomer actuator considering dynamic phase transition process," *IEEE Transactions on Cybernetics*, vol. 53, no. 7, pp. 4423–4434, 2023.
- [30] Y. Wang, X. Ma, Y. Jiang, W. Zang, P. Cao, M. Tian, N. Ning, and L. Zhang, "Dielectric elastomer actuators for artificial muscles: A comprehensive review of soft robot explorations," *Resources Chemicals and Materials*, vol. 1, no. 3, pp. 308–324, 2022. [Online]. Available: <https://www.sciencedirect.com/science/article/pii/S2772443322000447>
- [31] L. Wang, J. Lam, X. Chen, J. Li, R. Zhang, Y. Su, and Z. Wang, "Soft robot proprioception using unified soft body encoding and recurrent neural network," *Soft Robotics*, vol. 10, no. 4, pp. 825–837, 2023.
- [32] M. L. Anderson, R. Jing, J. C. P. Garcia, I. Yang, S. Alizadeh-Shabdiz, C. DeLorey, and A. P. Sabelhaus, "Maximizing consistent force output for shape memory alloy artificial muscles in soft robots," 2024.
- [33] X. Huang, K. Kumar, M. K. Jawed, A. Mohammadi Nasab, Z. Ye, W. Shan, and C. Majidi, "Highly Dynamic Shape Memory Alloy Actuator for Fast Moving Soft Robots," *Advanced Materials Technologies*, vol. 4, no. 4, p. 1800540, Apr. 2019. [Online]. Available: <https://onlinelibrary.wiley.com/doi/abs/10.1002/admt.201800540>
- [34] X. Huang, K. Kumar, M. K. Jawed, A. M. Nasab, Z. Ye, W. Shan, and C. Majidi, "Chasing biomimetic locomotion speeds: Creating untethered soft robots with shape memory alloy actuators," *Science Robotics*, vol. 3, no. 25, p. eaau7557, Dec. 2018. [Online]. Available: <http://robotics.sciencemag.org/lookup/doi/10.1126/scirobotics.aau7557>
- [35] Z. J. Patterson, A. P. Sabelhaus, K. Chin, T. Hellebrekers, and C. Majidi, "An Untethered Brittle Star-Inspired Soft Robot for Closed-Loop Underwater Locomotion," in *2020 IEEE/RSJ International Conference on Intelligent Robots and Systems (IROS)*, Oct. 2020, pp. 8758–8764.
- [36] S. Kennedy, M. R. E. U. Shougat, and E. Perkins, "Robust self-sensing shape memory alloy actuator using a machine learning approach," *Sensors and Actuators A: Physical*, vol. 354, p. 114255, 2023. [Online]. Available: <https://www.sciencedirect.com/science/article/pii/S0924424723001048>

- [37] S.-H. Lee and S.-W. Kim, "Improved position control of shape memory alloy actuator using the self-sensing model," *Sensors and Actuators A: Physical*, vol. 297, p. 111529, 2019. [Online]. Available: <https://www.sciencedirect.com/science/article/pii/S0924424719309409>
- [38] J. Prechtl, S. Seelecke, P. Motzki, and G. Rizzello, "Model-based, self-sensing actuator system based on antagonistic sma wires," in *ACTUATOR; International Conference and Exhibition on New Actuator Systems and Applications 2021*, 2021, pp. 1–4.
- [39] M. Ho and J. P. Desai, "Modeling, characterization and control of antagonistic SMA springs for use in a neurosurgical robot," in *2013 IEEE International Conference on Robotics and Automation*, May 2013, pp. 2503–2508.
- [40] S. S. Cheng, Y. Kim, and J. P. Desai, "Modeling and characterization of shape memory alloy springs with water cooling strategy in a neurosurgical robot," *Journal of Intelligent Material Systems and Structures*, vol. 28, no. 16, pp. 2167–2183, Sept. 2017. [Online]. Available: <https://doi.org/10.1177/1045389X16685443>
- [41] Y.-C. Pei, B.-H. Wang, J.-T. Wu, C. Wang, J.-H. Guan, and H. Lu, "A machine learning empowered shape memory alloy gripper with displacement-force-stiffness self-sensing," *IEEE Transactions on Industrial Electronics*, vol. 70, no. 10, pp. 10 385–10 395, 2023.
- [42] F. Simone, G. Rizzello, and S. Seelecke, "Metal muscles and nerves—a self-sensing sma-actuated hand concept," *Smart Materials and Structures*, vol. 26, no. 9, p. 095007, aug 2017. [Online]. Available: <https://dx.doi.org/10.1088/1361-665X/aa7ad5>
- [43] E. Ayvali and J. P. Desai, "Pulse width modulation-based temperature tracking for feedback control of a shape memory alloy actuator," *Journal of Intelligent Material Systems and Structures*, vol. 25, no. 6, pp. 720–730, Apr. 2014. [Online]. Available: <https://doi.org/10.1177/1045389X13502576>
- [44] A. P. Sabelhaus, R. K. Mehta, A. T. Wertz, and C. Majidi, "In-Situ Sensing and Dynamics Predictions for Electrothermally-Actuated Soft Robot Limbs," *Frontiers in Robotics and AI*, vol. 9, 2022. [Online]. Available: <https://www.frontiersin.org/article/10.3389/frobt.2022.888261>
- [45] A. Wertz, A. P. Sabelhaus, and C. Majidi, "Trajectory Optimization for Thermally-Actuated Soft Planar Robot Limbs," in *2022 IEEE 5th International Conference on Soft Robotics (RoboSoft)*, Apr. 2022, pp. 439–446.
- [46] *A Comparison of Mechanics Simplifications in Pose Estimation for Thermally-Actuated Soft Robot Limbs*, ser. Smart Materials, Adaptive Structures and Intelligent Systems, vol. ASME 2023 Conference on Smart Materials, Adaptive Structures and Intelligent Systems, 09 2023. [Online]. Available: <https://doi.org/10.1115/SMASIS2023-110774>
- [47] Y. Lu, R. Zhang, Y. Xu, L. Wang, and H. Yue, "Resistance Characteristics of SMA Actuator Based on the Variable Speed Phase Transformation Constitutive Model," *Materials*, vol. 13, no. 6, p. 1479, Jan. 2020. [Online]. Available: <https://www.mdpi.com/1996-1944/13/6/1479>
- [48] Z. J. Patterson, A. P. Sabelhaus, and C. Majidi, "Robust Control of a Multi-Axis Shape Memory Alloy-Driven Soft Manipulator," *IEEE Robotics and Automation Letters*, vol. 7, no. 2, pp. 2210–2217, Apr. 2022.
- [49] A. Koivikko, E. Sadeghian Raei, M. Mosallaei, M. Mäntysalo, and V. Sariola, "Screen-printed curvature sensors for soft robots," *IEEE Sensors Journal*, vol. 18, no. 1, pp. 223–230, 2018.
- [50] E. Olson, "Apriltag: A robust and flexible visual fiducial system," in *2011 IEEE international conference on robotics and automation*. IEEE, 2011, pp. 3400–3407.
- [51] A. P. Sabelhaus, Z. J. Patterson, A. T. Wertz, and C. Majidi, "Safe Supervisory Control of Soft Robot Actuators," Aug. 2022, arXiv:2208.01547 [cs, eess]. [Online]. Available: <http://arxiv.org/abs/2208.01547>
- [52] L. C. Brinson and M. S. Huang, "Simplifications and Comparisons of Shape Memory Alloy Constitutive Models," *Journal of Intelligent Material Systems and Structures*, vol. 7, no. 1, pp. 108–114, Jan. 1996. [Online]. Available: <http://journals.sagepub.com/doi/10.1177/1045389X9600700112>
- [53] E. Patoor, D. C. Lagoudas, P. B. Entchev, L. C. Brinson, and X. Gao, "Shape memory alloys, Part I: General properties and modeling of single crystals," *Mechanics of Materials*, vol. 38, no. 5-6, pp. 391–429, May 2006. [Online]. Available: <https://linkinghub.elsevier.com/retrieve/pii/S0167663605001195>
- [54] D. Hughes and J. T. Wen, "Preisach modeling of piezoceramic and shape memory alloy hysteresis," *Smart Materials and Structures*, vol. 6, no. 3, pp. 287–300, June 1997. [Online]. Available: <https://doi.org/10.1088%2F0964-1726%2F6%2F3%2F007>
- [55] C.-C. Lan and C.-H. Fan, "An accurate self-sensing method for the control of shape memory alloy actuated flexures," *Sensors and Actuators A: Physical*, vol. 163, no. 1, pp. 323–332, Sept. 2010. [Online]. Available: <http://www.sciencedirect.com/science/article/pii/S0924424710003511>
- [56] D. Cui, G. Song, and H. Li, "Modeling of the electrical resistance of shape memory alloy wires," *Smart Materials and Structures*, vol. 19, no. 5, p. 055019, Apr. 2010. [Online]. Available: <https://doi.org/10.1088/0964-1726/19/5/055019>
- [57] H. Kim, Y. Han, D.-y. Lee, J.-I. Ha, and K.-J. Cho, "Sensorless displacement estimation of a shape memory alloy coil spring actuator using inductance," *Smart Materials and Structures*, vol. 22, no. 2, p. 025001, Dec. 2012. [Online]. Available: <https://doi.org/10.1088/0964-1726/22/2/025001>
- [58] H. N. Bhargaw, B. A. Botre, S. Singh, S. A. R. Hashmi, S. A. Akbar, and P. Sinha, "Performance analysis of constant current heated antagonistic shape memory alloy actuator using a differential resistance measurement technique," *Smart Materials and Structures*, vol. 30, no. 12, p. 125031, Nov. 2021. [Online]. Available: <https://doi.org/10.1088/1361-665x/ac32e7>
- [59] R. J. Webster III and B. A. Jones, "Design and kinematic modeling of constant curvature continuum robots: A review," *The International Journal of Robotics Research*, vol. 29, no. 13, pp. 1661–1683, 2010.